

inhomogeneous particle distribution to prevent reinforcing particles from drifting apart by liquid metal during the casting process. But then, the decomposition of the binder at elevated temperatures would introduce gas production and other impurities, thereby porosity, slag and other serious defects may diminish the mechanical properties. Secondly, the key of WC particles as the reinforcing phase is the controlling of their size. Too fine of WC particles can readily dissolve in liquid iron and the resulting enhancement effect is not obvious; on the contrary, particles of a larger size can initiate crack and reduce the reinforcement effect, especially the fatigue property. Moreover, in order to reduce the particle drifting effect in the liquid iron, composite materials using the infiltration casting usually have a thickness of less than 10 mm. This largely limits the infiltration casting technique from applying to thicker wear-resistant parts.

In order to develop a new composite material for rolling mill guides, the feasibility of producing a uniform, about 15 mm thick and high hardness WC-Co particle reinforced high Cr cast iron based surface composites by the infiltration casting method without any binders was investigated. Based on the detailed studies of the microstructure evolution, hardness of the composite material and the interface characteristics, a composite layer formation mechanism was discussed.

1 Experimental procedure

Commercially available WC-8%Co particles with a size range of 2–6 mm (and with a hardness of 90 HRA and a density of $14.7 \text{ g}\cdot\text{cm}^{-3}$) were purchased as prefabricated reinforcement. The composite material was fabricated by a sand mold infiltration casting process. The WC-8%Co particles were placed at the bottom of the mold ($100 \text{ mm} \times 100 \text{ mm} \times 160 \text{ mm}$) with a height of 15 mm prior to casting. The riser was set at the top of the sand mold. High Cr cast iron with the chemical composition of Fe-24.7%Cr-1.73%C-1.68%Si-0.82%Ni (by weight) was poured into the mold at $1,560 \text{ }^\circ\text{C}$.

After infiltration and solidification, the casting block was cut along cross section to reveal the composite layer thickness. Furthermore, the volume fraction in the composite layer was determined using an optical microscope equipped with a

quantitative image analysis software package. The morphology and composition of the infiltrated composite were analyzed using scanning electron microscopy (SEM, JEOL-JSM5910), energy dispersive spectrometry (EDS), and electron probe microanalysis (EPMA). X-ray diffraction (XRD) was also used to determine the phase compositions in the composite material. The Rockwell hardness (both HRA and HRC) and microhardness were measured to determine the hardness profile in the composite material.

2 Results and discussion

2.1 Thickness of surface composite material

Figure 1 shows the macro-photograph of the composite material obtained by infiltration casting. No visual pores or significant inclusions are observed on the surface. The distinguishable boundary between the composite layer and high Cr cast iron matrix is clearly seen in Fig. 1(b). This strongly indicates that the reinforced particles are not re-positioned by the liquid metal during the casting process. The thickness of the composite layer is about 15 mm with an average density of $10.11 \text{ g}\cdot\text{cm}^{-3}$. The average volumetric fraction of the reinforced particles is evaluated to be 38% by density calculation method. These results indicate that the pressureless infiltration casting without any binders added can also produce quality composite materials. This phenomenon is ascribed to the available reinforced particles with suitable particle sizes. The WC-8%Co reinforced particles have a particle size range of 2–6 mm, enabling the liquid metal to infiltrate through the gaps among the dispersive particles under the combined gravity and capillary forces. Moreover, part of the Co from the reinforcements is dissolved into the matrix, enhancing the metallurgical bonding between the reinforced particles and the matrix materials.

2.2 Microstructure and hardness of surface composite material

The cross section of the composite material can be roughly divided into three layers: the particle reinforced metal matrix composite layer (PRMMCs layer), the transition layer and

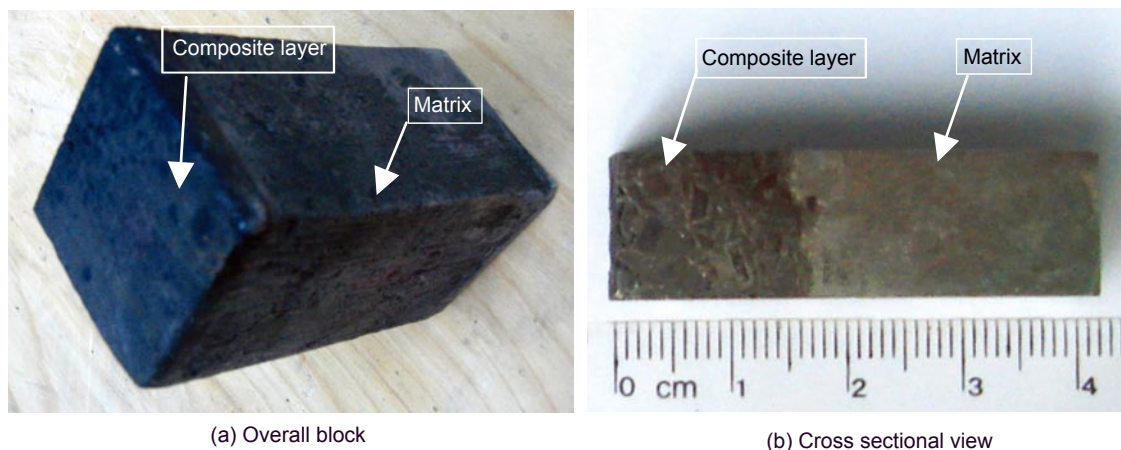


Fig. 1: Photographs of composite material sample prepared by infiltration casting

the matrix layer. Figure 2(a) presents the morphology of the PRMMCs layer, where the reinforced particles are distributed homogeneously in the high Cr cast iron matrix. Some small granular precipitations were found at the interfaces between the particles and matrix, as shown in Fig. 2(b). These precipitations contain high W and present the same color as that of the reinforced particles. Thereby, they are possibly the WC-Co tiny particles, and part of Co melt displaces and precipitates from the matrix during the cooling process. The formation of fine WC-Co particles further confirm the metallurgical bonding between the reinforced particles and the matrix material.

As shown in Fig. 2(c), a transition layer between the PRMMCs layer and the matrix layer is clearly determined. The transition layer mainly contains coarse dendrite, as shown in Fig. 3. This type of dendrite is different from the morphologies

of both matrix material in the matrix layer and that in the PRMMCs layer [Fig. 2(e), (f)]. Coarse dendrite usually suggests a localized high C content in the transition layer, which is probably due to the dissolving of WC particles into the matrix materials.

Figure 2(d) shows the reinforcing particle morphology inside the PRMMCs layer. In addition to rough blocks with pinholes, some smooth blocks are also observed within the particles. These dense blocks have fewer internal pores. This is ascribed to the melting of Co (m.p., 1,495 °C) at a high casting temperature, which results in the flowing of Co into the WC-Co particle and thus splicing the tiny WC particles to form dense blocks after solidification [10]. Pores are formed due to the capillary force of Co into the pores within WC grains during the liquid phase sintering process. Some bigger pores are formed by the co-

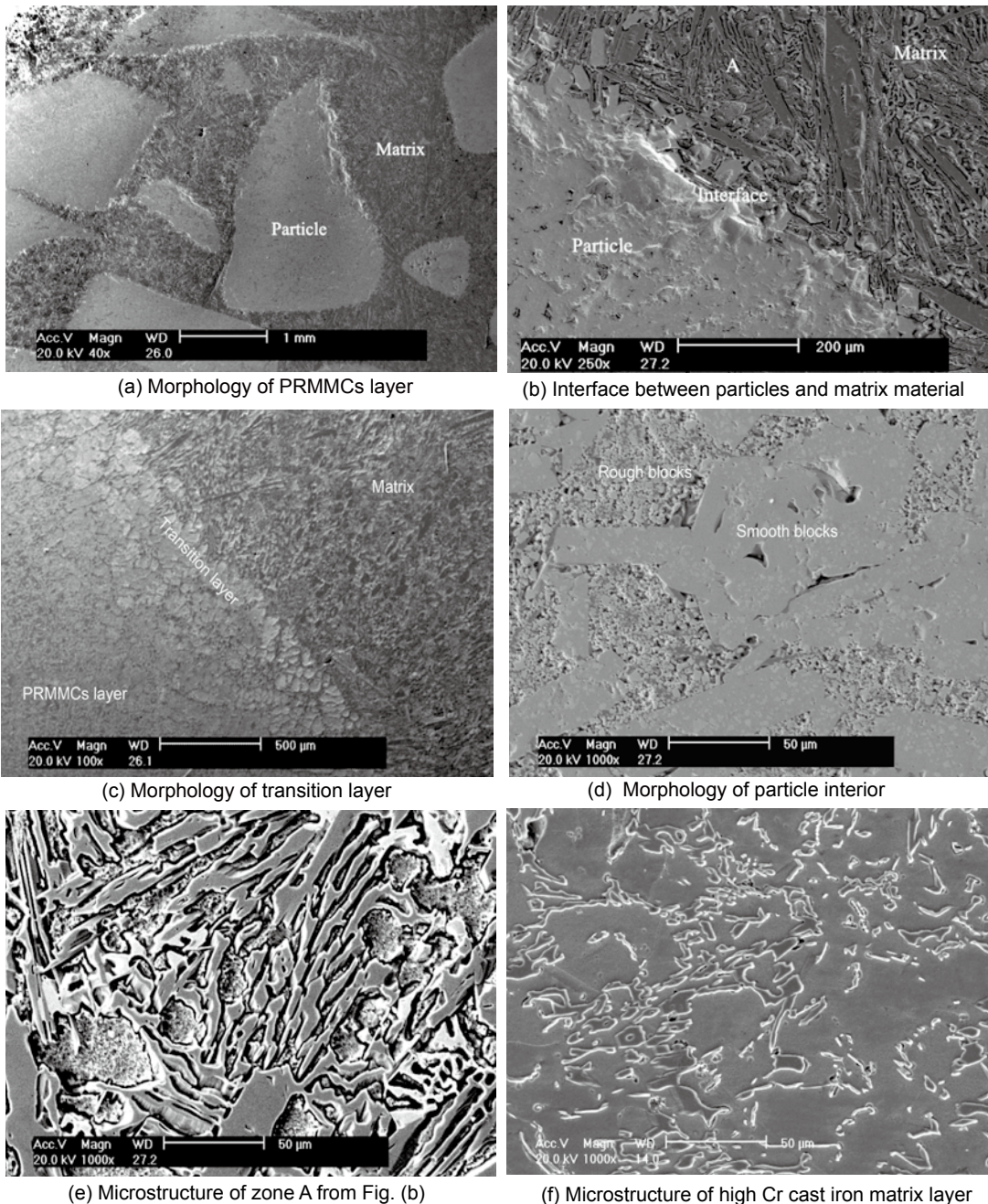


Fig. 2: Microstructure of WC-Co particle reinforced high Cr cast iron matrix surface composite material

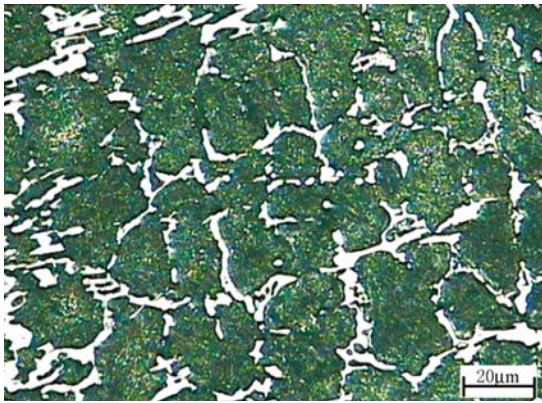


Fig. 3: Optical photograph of transition layer

Table 1: Chemical compositions at various zones inside composite material

Zone	Element (wt. %)			
	Fe	Cr	Co	W
The matrix inside the PRMMCs layer [Fig. 2(a) matrix]	52.8	23.3	1.9	22.0
The edge of the reinforcing particle [Fig. 2(b) interface]	22.0	7.6	4.7	65.7
The reinforcing particle interior [Fig. 2(d)]	18.2	5.7	3.7	72.4
The herringbone-like morphology inside the reinforcing particle [Fig. 2(e)]	34.1	27.6	1.4	35.5
The strip morphology inside the reinforcing particle [Fig. 2(e)]	26.7	53.4	1.2	12.8

effects of flowing resisting force, surface tension of the liquid metal and capillary action .

Figures 2(e) and (f) show the morphology of the matrix material inside the PRMMCs layer and the microstructure of high Cr cast iron matrix layer, respectively. Carbides with two morphologies (i.e. dark gray strip and gray herringbone-like) are observed in the PRMMCs layer. However, only a small amount of carbides are dispersed inside the matrix of the high Cr cast iron matrix layer. In addition, the average carbide size inside the PRMMCs layer is apparently greater than that inside the high Cr cast iron matrix layer, suggesting that WC particles partly dissolve into the matrix at elevated temperatures and raise the local C content. In addition, the dissolved W and C can react with other alloy elements such as Fe and Cr in the cast iron to form complex carbides, including $(Cr, W, Fe)_{23}C_6$, M_6C and $M_{12}C$ (where M represents Co, W, Fe), and precipitate in the subsequent cooling process.

Energy dispersive X-ray spectrometry (EDS) and X-ray diffraction (XRD) examinations evaluated the chemical variation and phase composition across the transition layer. The EDS results of various phases at different layers are summarized in Table 1, and the XRD patterns of high Cr cast iron matrix and PRMMCs layer are shown in Fig. 4 and Fig. 5, respectively.

The EDS results show that the W and Co contents respectively reach 22.0wt.% and 1.9wt.% in the matrix material inside the PRMMCs layer, confirming that W and Co are dissolved into

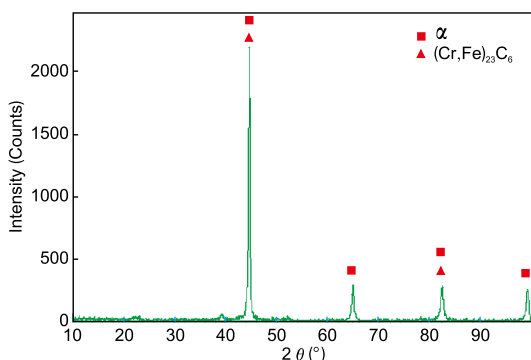


Fig. 4: XRD pattern from high Cr cast iron matrix layer

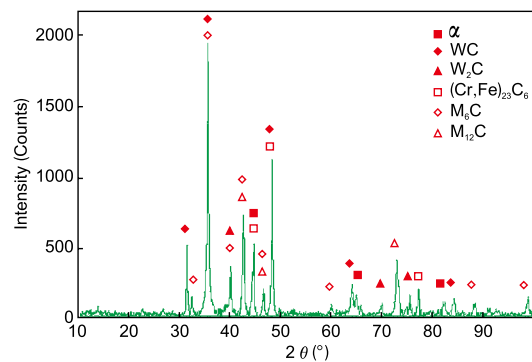
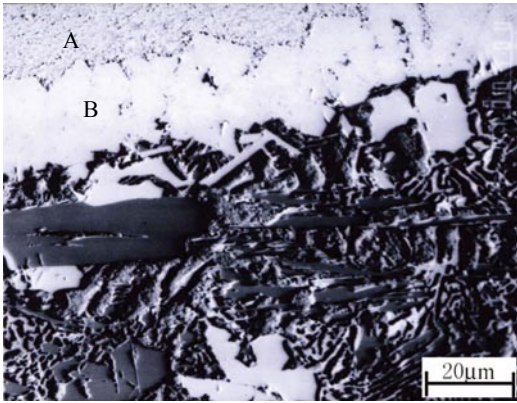


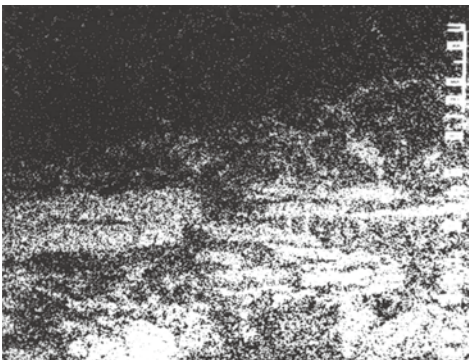
Fig. 5: XRD pattern from PRMMCs layer

the matrix materials during casting. The high Fe content of 18.2wt.% and Cr content of 5.7wt.% within the reinforcing particle inside indicates that Fe and Cr in the matrix materials diffuse into the reinforcing particle inside. Moreover, Fe, Cr, W elements demonstrate a gradient distribution from the reinforcing particle inside to the matrix material at the particle edge. The Co content is the highest at the edge of the particles, followed by that within the particles. The Co within the particles may transfer between WC particles after partial melting. That is why Co is poor within the particles [Fig. 2(d)]. Carbon content in the composite layer is obviously higher than that of base material layer. As analyzed above, this is the result of C atoms diffusing into the base material between particles after WC decomposed. The XRD pattern indicates that the high Cr cast iron matrix material is mainly composed of ferrite and a small amount of $(Cr, Fe)_{23}C_6$ carbides. The PRMMCs layer, however, contains not only the phases from the matrix materials but also other M_6C (Probably Fe_3W_3C and Co_3W_3C), $M_{12}C$ (Probably Fe_6W_6C and Co_6W_6C) and W_2C type complex carbides. These carbides likely correspond to the gray herringbone-like morphology. Due to their high Cr content, the $(Cr, W, Fe)_{23}C_6$ carbides are characterized by the dark gray strip morphology (Fig. 2(e)).

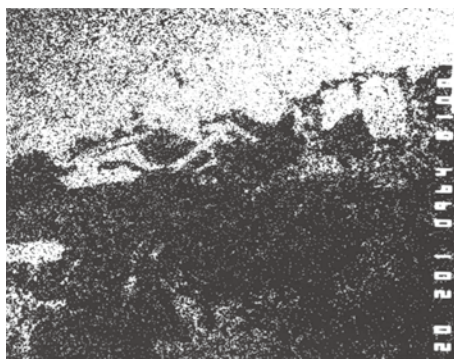
The main alloy element distribution close to the interface was characterized by electronic probe microanalysis (EPMA) as shown in Fig. 6. Figure 6(a) is the morphology near the interface.



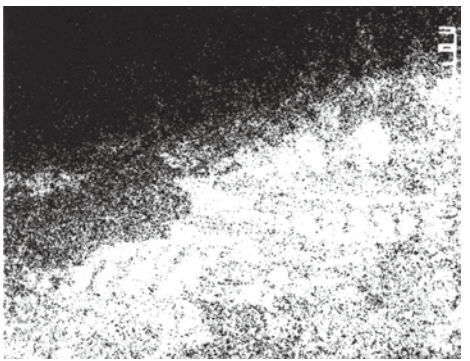
(a) Morphology near the interface



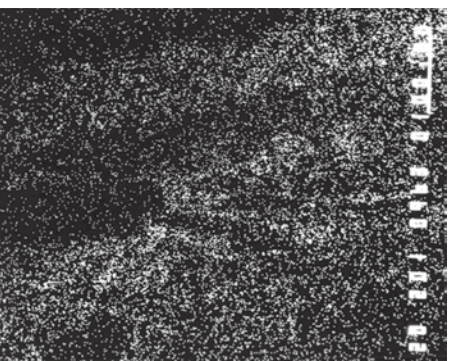
(b) Fe mapping images



(c) W mapping images



(d) Cr mapping images



(e) Co mapping images

Fig. 6: EPMA analysis results on interface between reinforcing particles and matrix material

Table 2: Hardness from different zones inside composite material

Zone	A	B	C	D	E	F
Macro-hardness (HRA)	86.3	81.5	80.9	74.3	67.0	66.5
Micro-hardness (HV _{0.3})	600-1800					

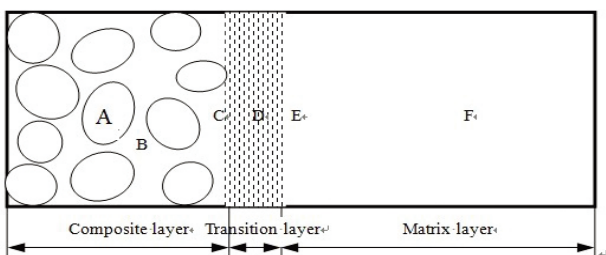


Fig. 7: Schematic hardness test zones on composite material surface

The white zone B represents the edge of the reinforcing particle, while zone A is located at the reinforcing particle interior. The element mapping images of Fe, W, Cr and Co are given in Fig. 6(b), (c), (d) and (e), respectively. The white area represents the corresponding element distribution. The migration of Fe and Cr from the matrix material to the reinforcing particle inside and the outflow of W and Co from the particle to the matrix materials could be clearly observed. These results are consistent with those from EDS. In particular, the flow of Co would result in the inhomogeneous distribution of Co element within the particle.

Table 2 shows the hardness test results. The macro-hardness (HRA) was evaluated by an average value of five measurements. The corresponding test zone schematic is shown in Fig. 7. The hardness value from zone A

represents the internal hardness of the reinforcing particles. The hardness from zone B is the hardness of the matrix material in the PRMMCs layer. Zone C, zone D and zone E represent the different locations near the transition layer. The hardness value of zone F is the average hardness of the matrix layer.

The macro-hardness and micro-hardness of original WC-Co prefabricated reinforcing particle are about 90 HRA and 1900 HV, respectively. But the macro-hardness of WC-Co particle in the composite layer is only 86.3 HRA, which is less than that of the original hardness of WC-8%Co particle (90 HRA). Micro-hardness changes more obviously, and the minimum value is only 600 HV. This could be attributed to the Co melting and dissolving in

molten high chromium cast iron at elevated temperatures. In particular, Co transferred after melting, causing the reduction in binder content between some WC particles and the decrease of bonding strength.

Figure 8(a) shows the internal metallographic morphology of WC-Co particles in the composite layer, in which there are a lot of "island" shape condensate blocks in the WC-Co particles. The low melting point Co would first melt at high temperature. While the whole WC-Co particle was in molten or semi-molten state, the molten Co could flow between the sintered WC particles, which could result in local parts becoming denser after solidification (as shown in Fig. 2(b) smooth block zones). Other parts (as shown in Fig. 2(b) rough block zones) become looser due to the reduced binder content. WC particles accumulate together with decreasing bonding strength and low hardness. The micro-hardness of density parts (about HV 1,800) could not reach the original hardness (HV 1,900). The melted Co and molten matrix iron diffuse from each

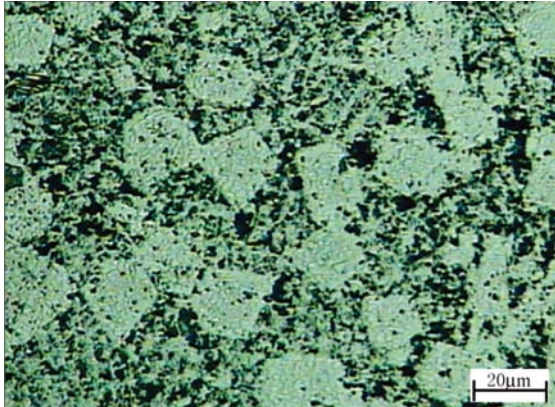


Fig. 8: Optical micrographs inside WC-Co ceramics particles

other may be the main reason, which changes the composition of binding phase inside WC-Co particles. A mixed phase composed of Fe, Cr, W, Co, C and related compound were formed after solidification. This structure was brittle and easily collapse or crushed under the pressure of hardness test head.

According to the above comprehensive analysis, the proposed composite is different from other types of iron base composites which were reinforced with WC and/or ceramic particles. In this study, WC-Co prefabricated particles with sizes of 2 – 6 mm were selected as the reinforcing phase. High Cr cast iron based surface composites were prepared with ordinary sand mold by casting infiltration method. The composite layer thickness was up to 15 mm approximately. The composite interface metallurgical bonding characteristics and microstructure/composition characteristics were investigated in the present study. It was found that Co was melted and dissolved, and a portion of WC was also dissolved into the WC-Co particle inside during the solidification process, which assisted the formation of composites like a link bridge between different phases. Atom diffusion contributed to the composite material sintering and solidification. The high hardness surface composites could be candidate materials for various conditions and applications

3 Conclusions

(1) The WC-Co particle reinforced high Cr cast iron composite material was prepared using a pressureless infiltration casting technique. The prefabricated reinforcing particles with a size of 2 – 6 mm are conducive to cast iron liquid infiltration. The obtained composite material possesses a composite layer of approximately 15 mm in thickness. The volumetric fraction of the reinforcing particles is 38%.

(2) During solidification, interface reaction took place between WC-Co particles and cast iron. Melting and dissolving

of prefabricated particles were found. Local Co melting and diffusion seem to play an important role in promoting interface metallurgical bonding. Fe and Cr migrate from the matrix material into the reinforcing particle interior, and W and Co flow out from the particles into the matrix material during the casting process, resulting in stronger metallurgical bonding interfaces between the matrix material and the reinforcing particles. The particle reinforced metal matrix composite layer contains not only these phases of ferrite and $(Cr, W, Fe)_{23}C_6$ from the matrix material but also other carbides such as WC, W_2C , M_6C and $M_{12}C$.

(3) The hardness distribution in the obtained composite material demonstrates a gradient decrease from the particle reinforced metal matrix composite layer to the matrix layer. The highest hardness of 86.3 HRA is obtained on the reinforced particle surface.

References

- [1] Jing Yehua, Zhou Rong, Lu Dehong, et al. Research on WC/cast iron Matrix surface-layer composites for slurry pump. Foundry, 2002, 51(3): 170-172. (In Chinese)
- [2] Hashim J, Looney L, Hashmi M S J. Particle distribution in cast metal matrix composites-Part I. Journal of Materials Processing Technology, 2002, 123(2): 251-257.
- [3] Niu Libin, Xu Yunhua, Wu Hong. Study on in-situ WC particles/tungsten wire reinforced iron matrix composites under electromagnetic field. China Foundry, 2010, 7(2): 158-162.
- [4] Zhong Lisheng, Xu Yunhua, Li Chengchen, et al. Infiltration casting and in situ fabrication of tantalum carbide particulate-reinforced iron matrix composites. Journal of Composite Materials, 2011, 46(8): 895-901.
- [5] Masayuki Mizumoto, Toshihisa Murano, Akio Kagawa. Microstructure control of particle reinforced metal matrix composites fabricated by low-pressure infiltration process. Materials transactions, 2002, 43(10): 2622-2634.
- [6] Li Xiubing, Gao Yimin, Xing Jiandong, et al. Producing WC particles reinforced grey cast iron matrix steel rolled guiding board in sand mold. Foundry Technology, 2004, 25(2): 95-96. (In Chinese)
- [7] Chen Yue, Shang Guanbao, Tie Xishun, et al. Research on wear-resistance property of WC/high-Cr cast iron composite layer. Foundry Technology, 2005, 26(10): 935-937. (In Chinese)
- [8] Wang Enze, Zheng Yanqing, Bao Chonggao, et al. Liquid-phase forming process for Al_2O_3 particle reinforced heat-resistant steel composite. Foundry, 1998 (3): 15-18. (In Chinese)
- [9] Kambakas K and Tsakirooulos P. Solidification of high-Cr white cast iron-WC particle reinforced composites. Materials Science and Engineering A, 2005, 413-414: 538-544.
- [10] ADAM Ana-Maria. Influence of rapid solidification on the microstructure of aluminium rich hypereutectic Al-Co alloys. U.P.B. Scientific bulletin, Series B: Chemistry and materials science, 2011,73(3): 217-228.